LANGMUIR



Interface Components: Nanoparticles, Colloids, Emulsions, Surfactants, Proteins, Polymers

# Soft Chemical Method for Synthesizing Intermetallic Antimonide Nanocrystals from Ternary Chalcogenide

Yilan Jiang, Long Yuan, Yanyan Xu, Jiaojiao Ma, Yu Sun, Xia Gao, Keke Huang, and Shouhua Feng

*Langmuir*, **Just Accepted Manuscript** • DOI: 10.1021/acs.langmuir.9b01774 • Publication Date (Web): 04 Nov 2019

# Soft Chemical Method for Synthesizing Intermetallic Antimonide Nanocrystals from Ternary Chalcogenide

Yilan Jiang[#], Long Yuan[#], Yanyan Xu, Jiaojiao Ma, Yu Sun, Xia Gao, Keke Huang[*], Shouhua Feng

State Key Laboratory of Inorganic Synthesis and Preparative Chemistry, College of Chemistry, Jilin University, Changchun 130012, People's Republic of China

Key Laboratory of Functional Materials Physics and Chemistry of the Ministry of Education, Jilin Normal University, Changchun 130103, People's Republic of China

**KEYWORDS:** Antimonide, Desulfurization, Synthesis, Ternary chalcogenide, Trialkylphosphine

**ABSTRACT:** The synthesis of intermetallic antimonides usually depends on either the high temperature alloying technique from high purity metals or the flux method in highly poisonous Pb-melt. In this paper, we introduced a soft chemical method to synthesize intermetallic antimonides from ternary chalcogenide precursors under argon atmosphere below 200 °C. Powder X-ray

diffraction and compositional analysis clearly indicate that a new phase of $Ag_3Sb$ nanocrystal was synthesized from the $Ag_3SbS_3$ precursors. Three types of trialkylphosphine (TAP) were applied as desulphurization agent and the transformation mechanism was elucidated. The capability of desulphurization agent is followed the sequence of triphenylphosphine (TPP) >tributylphosphine (TBP) >trioctylphosphine (TOP). Besides, this TAP-driven desulfurization route to synthesize intermetallic phase could also be possible for $AgSbSe_2$ and $Sb_2S_3$. Therefore, this paper provides an efficient mild technique for the fabrication of intermetallic nanocrystals.

## INTRODUCTION

Antimonide-based intermetallic phase compounds receive increasing concerns as important materials with interesting physical properties (such as superconductivity and half-metallity) and diverse structural chemistry of anionic substructures[1], that endow this family of materials potential applications in magnetic material[2], alloy-based anode materials for Li-ion batteries[3], catalysts[4], and thermoelectric materials[5]. Intermetallic antimonides are important members of nonclassic Zintl phases, which are intermediate between 2-center-2-electron with delocalized multicentre chemical bonding[6]. As one of the most important antimonide-based intermetallic phase compounds,

silver antimonides have been reported as anode materials for secondary lithium-ion batteries[7,8] and Pb-free solder alloys[9,10]. The alloy of antimonial silver has two members: dyscrasite ($Ag_3Sb$) and ε-phase of allargentum ($Ag_6Sb$). The last phase has been found in mineral that intimately intergrown with antimonial silver[11]. $Ag_3Sb$ is the primary exsolution phase from Ag-Sb liquid alloys according to a theoretical model[12].

The synthesis of intermetallic compounds is majorly dependent on the alloying technique by mixing high purity metal as starting materials at high temperature[13]. However, the stoichiometry of Ag/Sb varies dependent on the preparation temperature in alloying methods[14]. Single crystal of antimonide intermetallic compound could be synthesized by high vacuum solid state reaction[15], the microwave-assisted polyol process[16] and Sn- or Pb-flux method at over 900 °C[17,18]. High quality of $Ag_3Sb$ film has only been reported under ultra-high vacuum conditions via vapour epitaxy growth technique[19]. According to a previous study on the formation phase boundaries of $Ag_3Sb$, this phase is formed at 562 °C with controlled stoichiometry[20]. Kulifay reported a low temperature method for the synthesis of several intermetallic compounds via a route of reducing metal cations by $N_2H_4 \cdot 2HCl$ and $H_3PO_2$, however, the resulted products are usually impure with separated metal elements[21]. Zhao and Song et.al. have reported a chemical reduction route to synthesize Ag-Sb composite by

directly reducing the metal cations of $Ag^{+}$ and $Sb^{3+}$ by $NaBH_4$, however, it is difficult to control the degree of reductive reaction and mixed phases of Sb element and $Ag_3Sb$ was obtained[22]. Therefore, it still remains a great challenge to synthesize Sb-based intermetallic phase nanocrystal with a convenient method at ambient condition.

Metal cations in sulphides are more mobile than that of oxides due to the weak electronegativity of $S^{2-}$ than $O^{2-}$, which endows cation exchange reaction in-situ evolution in the crystal lattice for synthesizing new controllable mixed phase sulphide nanocrystals[22]. The phase selective extraction of Se and S from nanoscale metal chalcogenides by TOP has been reported as an effective strategy to synthesize less S,Se/metal ratio nanomaterials[23]. Recently, Yu et. al. report a TAP-driven chemical transformation route to synthesize a series nanostructures of Ag, Bi metal and mixed sulphide nanocrystals from Ag- or Bi-based sulphide precursors[25]. However, the research on the complete desulfurization of ternary Sb-based sulphide nanocrystals to synthetic $Ag_3Sb$ by cationic exchange has not been studied.

In our previous work, we have generally studied the synthesis of ternary Sb-based sulphide nanocrystals by hot-injection method with various phases and morphologies[26]. In this paper, we report a method to synthesize antimonide-based intermetallic

$Ag_3Sb$ nanocrystal by ternary sulphide nanocrystal. The conversion of $Ag_3Sb$ intermetallic nanocrystal from $Ag_3SbS_3$ was conducted in a mild condition at ambient pressure below 200 °C. PXRD and TEM results clearly indicate the desulfurization. Three types of TAP were applied as desulfurization agent and the transformation mechanism was elucidated. The capability of desulfurization agent is followed the sequence of TPP > TBP > TOP. Besides, the TAP-driven desulfurization method could also be used to retract metal phase from $AgSbSe_2$ and $Sb_2S_3$. The intermetallic phase extraction route illustrated in paper provides a fundamental understanding and practical method for synthesis of intermetallic nanocrystal.

## EXPERIMENTAL SECTION

**Chemicals.** Silver nitrate ($AgNO_3$, 99.8 %) was purchased from Sinopharm Chemical Reagent Co.Ltd. Sublimed sulfur (S, 99.5 %), selenium (Se, 99.9 %), oleylamine (OLA, 90 %), TPP, TBP and TOP were obtained from Aladdin. Antimony (III) trichloride ($SbCl_3$, 99.0 %), sodium diethyldithiocarbamatetrihydrate ( $Na(S_2CNEt_2) \cdot 3H_2O$, 98 %), 1-octa-decene (ODE, 90%) and oleic acid (OA, 90 %) were purchased from Alfa AesarCo., Inc. Hexane (99.7 %, A.R.) and ethanol (95.5 %, A.R.) were Beijing Chemical Industrial Group Co., Ltd. All chemicals were directly used without any further purification.

**Synthesis of $Sb(S_2CNEt_2)_3$ precursor.** $Sb(S_2CNEt_2)_3$ was prepared as followed procedure. 10 mmol of $SbCl_3$ and 30 mmol of $Na(S_2CNEt_2)\cdot 3H_2O$ were dissolved respectively in absolute ethanol. Then both of solutions were mixed and kept stirring for 30 min. The yellow precipitate was isolated through filtration, then washed with $H_2O$ and dried at 60 °C.

**Preparation of $Ag_3SbS_3$ nanocrystals.** The hot-injection route synthesis of $Ag_3SbS_3$ nanocrystals followed our previous work[27]. In a typical procedure, 3 mmol of $AgNO_3$, 1 mmol of $SbCl_3$ and 3 mmol S powders were added into a 100 mL three-necked flask containing ODE (8 mL), OLA (4 mL) and OA (2 mL) at room temperature. Then the mixture was degassed at 80-110 °C for removing water and the low boiling point impurities under vacuum for 20 min. The solution was heated up to 190 °C under an Ar atmosphere and kept for 1 h, during which the color of the mixture appeared yellow-orange. Then the resulting solution was cooled naturally at room temperature. Afterwards, $Ag_3SbS_3$ nanocrystals were dispersed and precipitated respectively using toluene and ethanol, and centrifugation was followed. The samples were purified several cycles and dried under vacuum condition.

**Preparation of $Ag_3Sb$ nanocrystals.** In order to obtain the $Ag_3Sb$ nanocrystals, 5 mL of OLA and 300μL (or 0.3 g) of TAP were added into the three-necked flask containing 25 mg of as-prepared

$Ag_3SbS_3$ nanocrystals at room temperature. Then the following procedure was same as that for the $Ag_3SbS_3$ nanocrystals.

**Preparation of $AgSbSe_2$ nanocrystals.** In a typical procedure, 1mmol of $AgNO_3$, 1 mmol of $SbCl_3$ and 2 mmol Se powders were added into a 100 mL three-necked flask containing ODE (8 mL), OLA (1 mL) and OA (1 mL) at room temperature. Then the mixture was degassed at 80-110 °C under vacuum for 20 min. The solution was heated up to 200 °C under an Ar atmosphere for 1 h. Then, the resulting solution was cooled naturally. Ethanol was added to precipitate the $AgSbSe_2$ nanocrystals and centrifugation was followed. The samples were purified several cycles by using toluene and ethanol, and dried under vacuum condition, finally.

**Chemical Transformation of $AgSbSe_2$ nanocrystals to $Ag_3Sb$ and Sb.** In a typical procedure, 25 mg of as-prepared $AgSbSe_2$ nanocrystals and 0.3g TPP were dispersed in 5 mL OLA in a 100 mL three-necked flask. The mixture was degassed at 90 °C and heated up to 190 °C under Ar and kept for 1 h.

**Preparation of $Sb_2S_3$ nanocrystals and desulfurize to Sb.** The above mentioned $Ag_3SbS_3$ experimental procedure was also followed for the prepare of $Sb_2S_3$ nanocyrstals, except that the material was $Sb(S_2CNEt_2)_3$ and the solvent ratio was tuned to OLA:OA:ODE= 2:1:2. The desulfurization process for $Sb_2S_3$ nanocrystals is followed the same procedure as that of $AgSbSe_2$.

**Characterization.** The crystal structures of the as-prepared products were investigated by powder X-ray diffraction (XRD, D/MAX2550, Rigaku, Japan) with graphite monochromic Cu Kα radiation. The 2θ range was 10-80°, and the scan speed was 3°/min. The microstructures were characterized by transmission electron microscopy (TEM, Tecnai G2S-Twin F20, FEI, Holland) and the scanning electron microscopy (SEM, Helios NanoLab 600i, FEI, Holland). X-ray photoelectron spectra (XPS) were acquired to analyze the surface composition of materials with an ESCALAB 250Xi electron energy spectrometer from Thermo company, and Al Kα (1486.6 eV) served as the X-ray excitation source.

## RESULTS AND DISCUSSION

**Synthesis of $Ag_3Sb$ by desulfurization from ternary sulfide $Ag_3SbS_3$ nanocrystals.** $Ag_3SbS_3$ precursor nanocrystals were synthesized follows our previous work.[27] Intermetallic $Ag_3Sb$ nanocrystals were obtained by treated $Ag_3SbS_3$ with various TAP solutions. As shown in Figure 1, $Ag_3SbS_3$ presents the typical diffraction peaks of trigonal structure (pyrargyrite phase with JCPDS card No. 74-1875) and the the space group of it is R 3c. After been treated with TPP for 1 h, S in $Ag_3SbS_3$ was removed to form $Ag_3Sb$. The as-synthesized $Ag_3Sb$ shows a high purity phase. The diffraction peak positions and their intensities match well

with the simulated pattern of orthorhombic structure of $Ag_3Sb$ (simulated from a CIF file with ICSD #52600). The space group of $Ag_3Sb$ is Pmmn with its lattice parameter of a=5.99 Å, b=4.85 Å, c=5.24 Å,

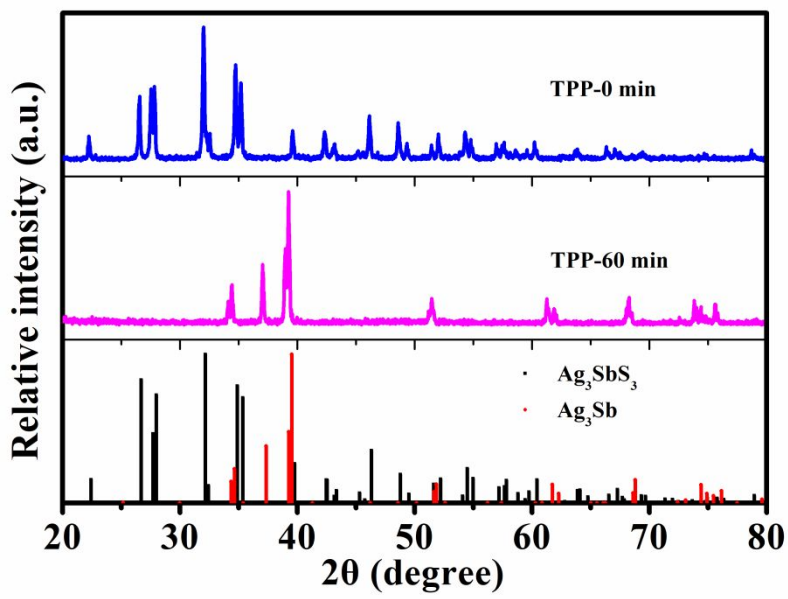


**Figure 1.** PXRD pattern of TPP-0 min and TPP-60 min.

respectively. No distinguishable diffraction peaks from secondary phases of Ag- or Sb-species could be observed in the XRD patterns of the pattern, suggesting that the as-synthesized $Ag_3Sb$ nanocrystals are pure phase.

Shown in Figure 2a is the SEM graph of $Ag_3SbS_3$ while Figure 2b is as-synthesized $Ag_3Sb$ nanocrystals obtained by TPP treatment. The size of $Ag_3Sb$ is larger than that of $Ag_3SbS_3$ nanocrystals and no definite morphology for each $Ag_3Sb$ nanocrystals, which is due to the imbalance in different treatment conditions of TAP

solutions and reaction temperatures. The EDS results show that the obtained sample contains only two elements, Ag and Sb, and the atomic ratio of the two elements is about 3:1, indicating that pure $Ag_3Sb$ is obtained.

High-resolution XPS spectra of Ag 3d and Sb 3d for the as-prepared $Ag_3Sb$ sample are obtained using C 1s as the reference at 284.6 eV, as shown in Figure 3. Peaks of Ag $3d_{3/2}$ and $3d_{5/2}$ of $Ag_3Sb$ locate at 374.05 and 368.02 eV, respectively, which is higher than that of

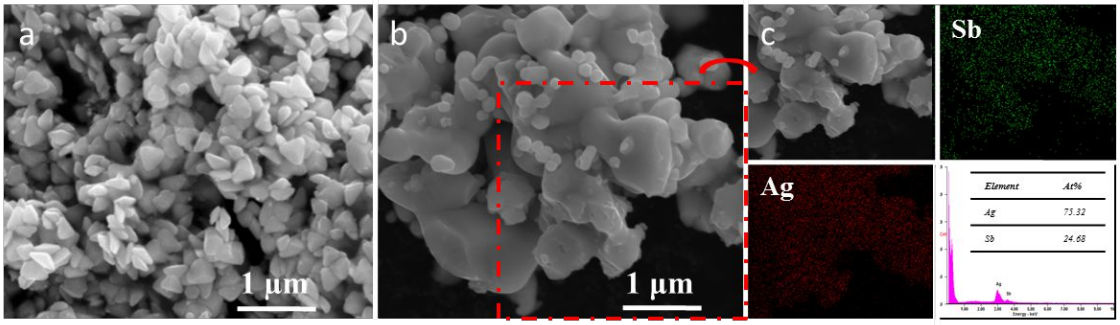


**Figure 2.** (a) SEM image of $Ag_3SbS_3$, (b) SEM image of $Ag_3Sb$, (c) EDS of $Ag_3Sb$ obtained by TPP treated $Ag_3SbS_3$ nanocrystal precursors.

$Ag_3SbS_3$ (373.9 eV for Ag $3d_{5/2}$ and 367.8 eV for Ag $3d_{3/2}$). Also, the binding energy peaks for Sb of $Ag_3Sb$ is higher than $Ag_3SbS_3$, which is located at 539.60 and 530.30 eV for Sb $3d_{5/2}$ and Sb $3d_{3/2}$, respectively. On the one hand, these results indicate a nearly zero valance state of Ag and Sb as an intermetallic phase of the as-synthesized compound.[28] On the other hand, we can also

learn that the bonding force between Ag and Sb is enhanced after desulfurization.

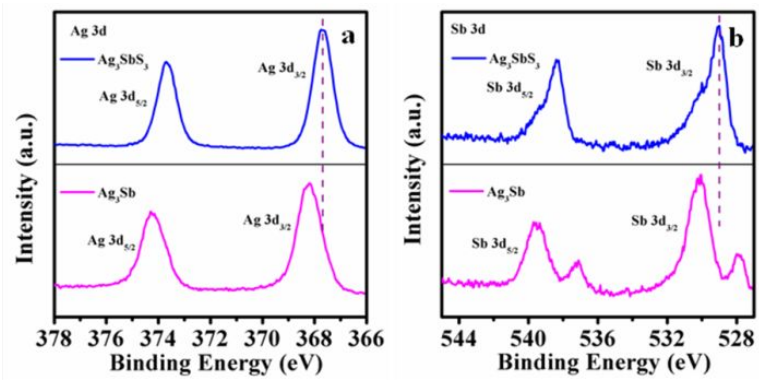


**Figure 3.** XPS spectra of $Ag_3Sb$ with the element binding energy of Ag 3d and Sb 3d, respectively.

**Effect on Desulfurization.** Three types of TAP (i.e. TOP, TPP and TBP) were adopted to desulfurize from ternary sulfide $Ag_3SbS_3$ nanocrystal precursors with various treatment time. When ternary sulfide treated in TOP for 10 min (TOP-10 min), the XRD pattern shows that it remains $Ag_3SbS_3$ (JCPDS card No. 74-1875) with a weak sign of getting $Ag_3Sb$ as shown in

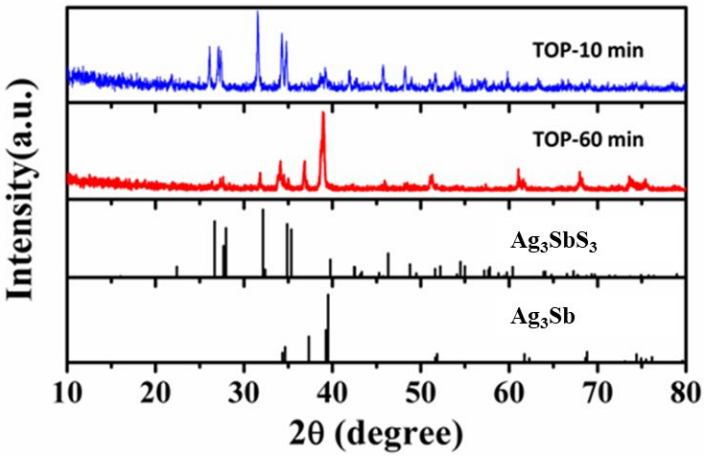


**Figure 4.** Treatment time of TOP on the formation of $Ag_3Sb$.

Figure 4. When been treated with TOP up to 60 min (TOP-60 min), a clear set of diffraction peaks of $Ag_3Sb$ phase is shown with a slight amount of $Ag_3SbS_3$ phase, which indicates that the sulfur in $Ag_3SbS_3$ nanocrystal has been etched from the ternary sulfide crystal lattice with the assistance of TOP molecule.

SEM graphs of $Ag_3SbS_3$ nanocrystals treated by TOP show clear particle size reduction due to the selective removal of S from $Ag_3SbS_3$ lattice (Figure 5). The particle size (c.a. 200 nm in length) and shape of TOP-10 min is near with that of as-synthesized $Ag_3SbS_3$ nanocrystals. For the samples treated for 60 min, however, the particle size of TOP-60 min is c.a. 50 nm. Nanorod morphology in the SEM graphs of Figure 5 is also ascribed to the $Ag_3Sb$ phase, because of no secondary phase could be determined from PXRD results. According to Bravais-Friedel-Donnay-Harker theory, crystal growth speed along different directions is proportional to the inverse of crystal lographic plane distances, i.e. the smallest $d_{hkl}$ value position of (010) is 18.49°, with a $d_{010}$ of 4.85 Å, grow the fastest that will diminish in the final crystal morphology[29,30]. While the peak position of (100) and (001) locates at 14.78° and 16.91°, which corresponded to a $d_{100}$ and $d_{001}$ value of 5.99 and 5.24 Å. This structure characteristic of $Ag_3Sb$ indicates a

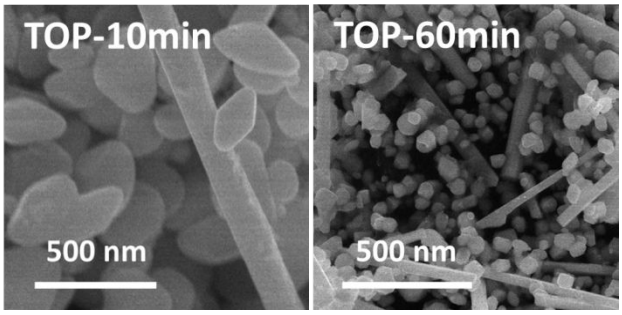


**Figure 5.** SEM of $Ag_3Sb$ obtained by TOP treated $Ag_3SbS_3$ nanocrystals with different times of 10 min and 60 min, respectively.

preferential growth orientation is <010> direction with the retard growth along <001> and <100>, that may lead to a rod-like morphology of the ideal growth in final products.

For comparison, the same ternary sulfide nanocrystal sample was also treated with TBP for 60 min (TBP-60 min) as shown in Figure 6. Combined with the XRD spectrum of TPP-60 min, it can be seen that pure phase of $Ag_3Sb$ could be obtained via both TPP and TBP solvent. Also, SEM graph of TBP-60 min is shown in the inset of Figure 6. Compared with the particle size of TPP-60 min, which shown in Figure 2b, TBP-60 min is smaller. Average particle size of TPP-60 min and TBP-60 min is 350 nm and 172 nm, respectively, which is much larger than that of TOP-60 min. Both of the $Ag_3Sb$ samples show no definite shape of crystal, which may due to the imbalance in ion diffuse in the TAP solvents.

Moreover, we used TPP to treat $Ag_3SbS_3$ for 15, 30, 45, 60 min to better explore the effects of samples over time. This is because the sample obtained by TPP is the most easily observed due to since the obtained samples is larger than others. According to the PXRD pattern from Figure S1, we can see that the phase of $Ag_3Sb$ appears when treated with TPP for 15 min. The phase of $Ag_3SbS_3$ is completely converted to phase $Ag_3Sb$ at 30 minutes. Continue to extend the time of TPP processing, $Ag_3Sb$ phase remains unchanged. As shown in Figure S2, the particle

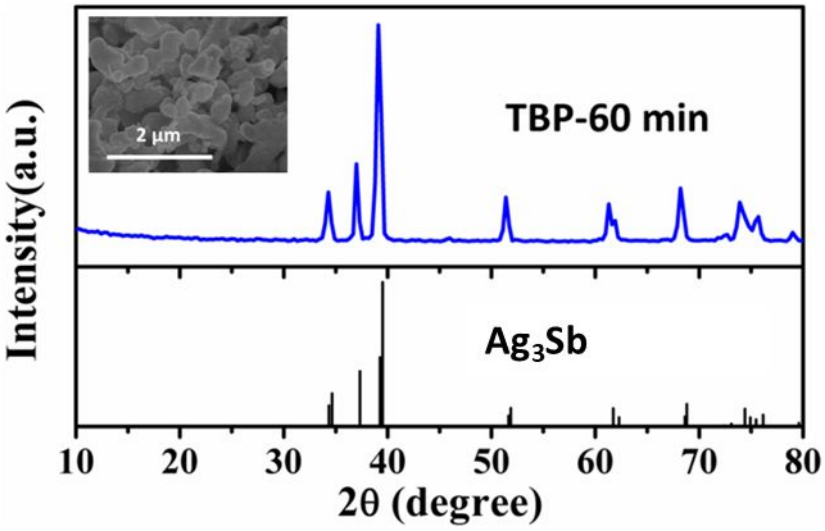


**Figure 6.** PXRD of $Ag_3Sb$ which obtain by treated $Ag_3SbS_3$ with TBP for 60min and the inset is the SEM image of TBP-60 min.

size and shape of $Ag_3SbS_3$-TPP-15 min are similar to that of as-synthesized $Ag_3SbS_3$ nanocrystals. When been treated for 30 minutes, the sample gradually became larger and a rod-like structure appeared, which was similar to the sample treated with

TOP. The SEM images of the obtained $Ag_3Sb$ nanocrystals show significant aggregation as the treatment time continue to extend (Figure S2). High-resolution XPS spectra of Ag 3d, Sb 3d and S 2p for the samples are obtained using C 1s as the reference at 284.6 eV, as shown in Figure S3. After $Ag_3SbS_3$ is treated with TPP, the peaks of Ag and Sb gradually move toward higher binding energy, indicating that the bonding force between Ag and Sb is enhanced, and the peak of S gradually disappears, indicating of the process of desulfurization.

To check the effectiveness of the method to synthesize $Ag_3Sb$ intermetallic phase nanocrystal, we also applied this method to treat $AgSbSe_2$ nanocrystals. As shown in Figure S4a, PXRD result show the $AgSbSe_2$ is pure phase (JCPDS #12-0379). After been treated with TPP for 60 min, it shows clear evidence of the deselenium from ternary chalcogenide phase with the main product of $Ag_3Sb$ and some impurity of Sb element (JCPDS card No. 35-0732). Shown in Figure S4b is the SEM image of $AgSbSe_2$, the rod-like shape is obtained by the synthetic method. However, $Ag_3Sb$ sample obtained from $AgSbSe_2$ shows no definite shape of crystal (Figure S4c), which may due to the imbalance in ion diffuse in the TPP solvents. The desulfurization effect is also possible shown in TPP treated $Sb_2S_3$ as shown in Figure S5. The primary synthesized $Sb_2S_3$ shows the typical diffraction peaks of

orthorhombic structure (JCPDS #42-1393) and the space group of it is Pbnm (Figure S5a). After treated with TPP for 60 min, it changes into trigonal structure (space group is R 3m), which corresponded to Sb phase (JCPDS #42-1393). SEM images in Figure S6 show that the samples agglomerated before and after treatment, and the size of ions decreased slightly after treatment. This result indicates that the de-chalcogenide method by TAP could be applied to synthesize most of Sb-based intermetallic alloys from their multi-chalcogenide precursors.

**Mechanism for desulfurization from ternary sulfide.** In order to understand the mechanism of desulfurization effect of TAP from ternary sulfide nanocrystal, the molecule structure and function should be analyzed in advance. In our experiment, three types of TAP have been used to etch $S^{2-}$ or $Se^{2-}$ from $Ag_3SbS_3$ and $AgSbSe_2$ precursors. They are all characterized with 4 $sp^3$ hybrid orbitals with 3 of them bonded with different alkyl groups, i.e. butyl-, octyl- and phenyl-group. The un-bonded orbital of P is occupied with one pair of lone electrons, which endows the reductive properties of TAP in most of chemical reactions. TOP has been regarded as an promoter to enhance cation exchange processes due to its strong binding affinity to Cu(I)[31]. The desulfurization capability of TAP is mainly dependent on this binding effect to Ag and Sb in the ternary chalcogenide in our experiment. Factors

that determine the capability of TAP are dominated by the alkyl group that bonding to center P-atom through steric hindrance effect and

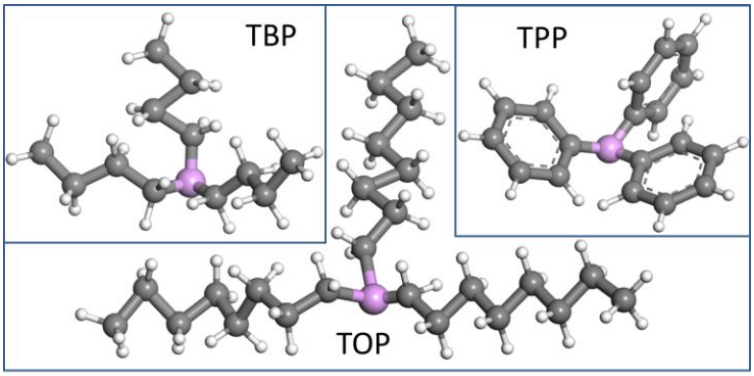


**Figure 7.** Molecule structure of three types of TAP.

charge transfer effect. Octyl-group is a long chain of $-(CH_2)_7-CH_3$, which may hinder the interaction between the sole pair electrons of $sp^3$ hybrid P with Ag or Sb in the crystal lattice of $Ag_3SbS_3$. Phenyl-group is a phenyl ring with delocalized electrons from conjugated orbital of the $sp^2$ hybrid C atoms, which may provide additional electrons that could transfer to the orbital of $sp^3$ hybrid P atom to increase its electron negativity and binding affinity to metal cations in ternary chalcogenide nanocrystals. Butyl-group is a short akyl-chain of $-(CH_2)_3-CH_3$, that neither such strong steric effect to lower its affinity, nor electron transfer effect to increase its negativity.

According to the desulfurization process in our experiment, the strongest desulfurization agent of TAP is TPP, followed by

TBP, and weakest TOP. For the same $Ag_3SbS_3$ nanocrystal precursor treatment with same time, TPP results in poorly crystalized $Ag_3Sb$; TBP results in the samples with good crystallinity; and TOP results in the mixture of unreacted $Ag_3SbS_3$ and $Ag_3Sb$ intermetallic phase. In order to understand the transformation mechanism from $Ag_3SbS_3$ to $Ag_3Sb$, ex-situ TEM was measured for the untreated $Ag_3SbS_3$ and treated samples with increasing time from 10 min to 4 h as shown in Figure 8. $Ag_3SbS_3$ sample with the initial morphology of tetrahedral shape nanocrystals was used to discriminate the morphology evolution process. Typical tetrahedral structure shape nanocrystal with rounded corners is shown in Figure 8a. The surface of the nanocrystal is smooth without any other particle attachment. After this sample is treated with TOP for 10 min, small particles were grown on the surface of the $Ag_3SbS_3$ nanocrystal, which can be seen in Figure 8b marked with red circle. The $Ag_3Sb$ phase grows gradually with the increasing the interaction between TOP and $Ag_3SbS_3$ that induced to a rod morphology of the intermetallic phase (Figure 8c). After treatment of $Ag_3SbS_3$ in TOP for 4 h, the shape of $Ag_3Sb$ is consisted with long nanorod and small nanoparticles (Figure 8d). These results are in agreement with the PXRD in previous discussions of this paper. In addition, HRTEM results of $Ag_3SbS_3$ show typical (211) and (110) crystal plane distances

of 0.33 and 0.55 nm, respectively, (Figure 8e) while $Ag_3Sb$ shows (021) and (200) crystal plane

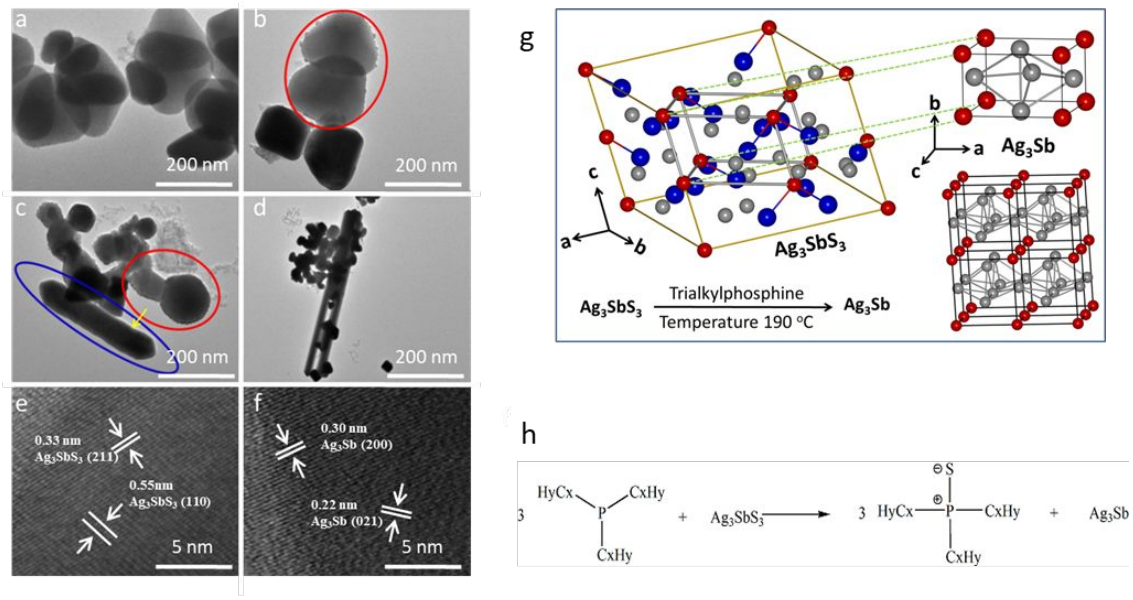


**Figure 8.** Ex-situ TEM graphs of time dependent desulfurization processes from $Ag_3SbS_3$ to $Ag_3Sb$ treated in TOP. (a) $Ag_3SbS_3$ nanocrystal, $Ag_3SbS_3$ treated with TOP for (b) 10 min, (c) 1 h, and (d) 4 h, respectively. Red circles in (b) and (c) are indicated to show the $Ag_3Sb$-decorated $Ag_3SbS_3$ nanocrystals. Blue circle indicates the formation of $Ag_3Sb$ rod after treatment with TOP for 1 h. (e) HRTEM of $Ag_3SbS_3$ (f) HRTEM of TOP-60 min, (g) Schematic of the transformation process from $Ag_3SbS_3$ to $Ag_3Sb$ by the desulfurization effect of TAP. Ag: grey balls; Sb: red balls; S: blue balls. (h) Reaction of TAP with $Ag_3SbS_3$.

distances of 0.22 and 0.30 nm, respectively. (Figure 8f) In comparison, the chemical formula of $Ag_3SbS_3$ and $Ag_3Sb$ could simply subtract S from the former compound.

For clarity, the crystal unit cell structure of $Ag_3SbS_3$ and $Ag_3Sb$ were plotted in Figure 8g. $Ag_3SbS_3$ is known as the mineral name of pyrargyrite that crystalized into a trigonal crystal system with a space group of R 3c (161). In each unit cell of $Ag_3SbS_3$, there are six $Ag_3SbS_3$ isolated unit with Sb occupied at 6a-site, Ag 18b-site and S 18b-site in Wyckoff's position system. The bond length is 2.4609 Å for Sb-S, and 2.4249 Å and 2.4613 Å for Ag-S, respectively. In the lattice of $Ag_3SbS_3$, Sb atoms mainly occupied at the corner of each unit cell with the other Sb and Ag inserted that weakly bonded with $S^{2-}$ nominally. With the assistance of the desulfurization from TAP, S is getting removed from the lattice of $Ag_3SbS_3$, and the remaining metal atoms crystalized into an intermetallic phase of $Ag_3Sb$ simultaneously. The crystal structure of $Ag_3Sb$ is orthorhombic with a space group of Pmmn. The position of Sb in $Ag_3Sb$ lattice is also at the corner of the unit cell (1a-site in Wyckoff's notation), with three sites for Ag atoms inside of the crystal lattice, which could be found as a primary model from $Ag_3SbS_3$ lattice with slightly adjustment of the crystal lographic position after S extraction. Therefore, the transformation from $Ag_3SbS_3$ to $Ag_3Sb$ with the assistance of TAP is possible. Reaction

of TAP with $Ag_3SbS_3$ is showed in Figure 8h. Combined with previous research,[32-35] we speculate that TAP react with $Ag_3SbS_3$ to give trialkylphosphane sulfide by elimination of one alkyl substituent, and $Ag_3Sb$ generated at the same time.

## CONCLUSIONS

In summary, we have performed the first example of transformation of ternary antimonite chalcogenide into intermetallic phase by the extraction effect of TAP under Ar atmosphere below 200 °C. Powder x-ray diffraction and compositional analysis clearly indicate that a new phase of $Ag_3Sb$ nanocrystal was synthesized from the $Ag_3SbS_3$ precursors. Three types of TAP were applied as desulfurization agent and the transformation mechanism was elucidated. The capability of desulfurization agent is followed the sequence of TPP > TBP > TOP. Besides, this TAP-driven desulfurization route to synthesize intermetallic phase could also be possible for $AgSbSe_2$ and $Sb_2S_3$. This paper illustrates an efficient and safe technique for the preparation of intermetallic nanocrystals.

## ASSOCIATED CONTENT

**Supporting Information.**

Additional information including PXRD, SEM and of treatment time of TPP on the formation of $Ag_3Sb$. PXRD result and SEM graph of octahedral shape $Ag_3Sb$ nanocrystal from the deselenium of $AgSbSe_2$. PXRD and SEM graph of $Sb_2S_3$ and desulfurized phase of $Sb_2S_3$ nanocrystals.

## AUTHOR INFORMATION

### Corresponding Author

*E-mail: kkhuang@jlu.edu.cn

### Notes

The authors declare no competing financial interest.

## ACKNOWLEDGMENT

This work was supported by the National Natural Science Foundation of China (Grant Nos. 21671076, 21427802).

### Author Contributions

# Y. Jiang and L. Yuan contributed equally to this work.

## REFERENCES

(1) Mills, A. M.; Deakin, L.; Mar, A. Electronic Structures and Properties of $RE_{12}Ga_4Sb_{23}$ (RE = La-Nd, Sm) and Superconducting $La_{13}Ga_8Sb_{21}$. *Chem. Mater.* **2001**, *13*, 1778-1788.

(2) Chen, X.; Shen, J. N.; Wu L. M.; Chen, L. A Ferrimagnetic Zintl Phase $Pr_4MnSb_9$: Synthesis, Structure, and Physical Properties. *Inorg. Chem.* **2013**, *52*, 7441-7447.

(3) Park, C. M.; Kim, J.-H.; Kim, H.; Sohn, H.-J. Li-alloy based anode materials for Li secondary batteries. *Chem. Soc. Rev.* **2010**, *39*, 3115-3141.

(4) Bauer, J. C., Chen, X.; Liu, Q.; Phan, T. H.; Schaak, R. E. Converting nanocrystalline metals into alloys and intermetallic compounds for applications in catalysis. *J. Mater. Chem*. **2008**, *18*, 275-282.

(5) Tan, G.; Zhao, L. D.; Kanatzidis, M. G. Rationally Designing High-Performance Bulk Thermoelectric Materials. *Chem. Rev*. **2016**, *116*, 12123-12149.

(6) Xia S. Q.; Bobev, S. Cation-Anion Interactions as Structure Directing Factors: Structure and Bonding of $Ca_2CdSb_2$ and $Yb_2CdSb_2$. *J. Am. Chem. Soc*. **2007**, *129*, 4049-4057.

(7) Vaughey, J. T.; Fransson, L.; Swinger, H. A.; Edström, K.; Thackeray, M. M. Alternative anode materials for lithium-ion batteries: a study of $Ag_3Sb$. *J. Power Sources*. **2003**, *119-121*, 64-68.

(8) Zhang,W. J. A review of the electrochemical performance of alloy anodes for lithium-ion batteries. *J. Power Sources.* **2011**, *196*, 13-24.

(9) Masson, D. B.; Kirkpatrick, B. K. Equilibrium solidification of Sn-Ag-Sb thermal fatigue-resistant solder alloys.*J. Electron. Mater.***1986**, *15*, 349-353.

(10) Lee, H. T.; Chen, M. H.; Jao, H. M.; Hsu, C. J. Effect of adding Sb on microstructure and adhesive strength of Sn-Ag solder joints. *J. Electron. Mater*. **2004**, *33*, 1048-1054.

(11) Somanchi, S.; Clark, L. A. The occurrence of $Ag_6Sb$ phase at Cobalt, Ontario. *The Canadian Mineralogist*. **1966**, *8*, 610-619.

(12) Singh, B. P.; Adhikari, D.; Jha, I. S. Concentration dependence of the structure and thermodynamic properties of silver–antimony alloys. *J. Non-Crystalline Solids*. **2010**, *356*, 1730-1734.

(13) Ruan, Y.; Wang, N.; Cao, C.; Wei, B. Rapid solidification mechanism of $Ag_{60}Sb_{34}Cu_6$ ternary alloy in drop tube. *Chin. Sci. Bull*. **2004**, *49*, 1801-1805.

(14) Somanchi,S. Subsolidus phase relations in the system Ag-Sb. *Canadian J. Earth Sci.* **1966**, *3*, 211-222.

(15) Zheng,W. Z.; Wang, P.; Wu, L. M.; Chen, L. Synthesis, Crystal and Electronic Structures, and Physical Properties of Caged Ternary Cu-Rich Antimonide: $BaCu_{7.31(3)}Sb_5$. *Inorg. Chem.* **2010**, *49*, 7491-7496.

(16) Teichert, J.; Heise, M.; Chang, J. H.; Ruck, M. Refinement of the Microwave - Assisted Polyol Process for the Low - Temperature Synthesis of Intermetallic Nanoparticles. *Eur. J. Inorg. Chem.* **2017**, *42,* 4930–4938

(17) Hu, Y.; Chen, C. W.; Cao, H.; Makhmudov, F.; Grebenkemper, J. H.; Abdusalyamova, M. N.; Morosan, E.; Kauzlarich, S. M. Tuning Magnetism of $[MnSb_4]^{9-}$ Cluster in $Yb_{14}MnSb_{11}$ through Chemical Substitutions on Yb Sites: Appearance and Disappearance of Spin Reorientation. *J. Am. Chem. Soc.* **2016**, *138*, 12422-12431.

(18) Zhu, M.; Tan, W.; Wu, Z.; Tao, X. T.; Huang, B.; Xia, S. Q. $Sr_4Cu_{25.37(18)}Sb_{12}$ and $Eu_4Cu_{26.06(13)}Sb_{12}$: Copper-Rich AntimonideIntermetallics with Cage Structure. *Cryst. Growth Des.* **2018**, *18*, 1722-1729.

(19) Gardiner, T. M.; Stiddard, M. H. B. Epitaxial growth and stabilization of the compound $Ag_3Sb$ on silver {1 1 1}. *J. Mater. Sci.* **1981**, *16*, 1522-1526.

(20) Feschotte, P.; Monachon, F.; Durussel, Ph. The binary system Sb-Ag: a revision of the $Ag_3Sb$ phase boundaries. *J. Alloy Comp*. **1992**, *186*, L17-L18.

(21) Kulifay,S. M. A Low Temperature Synthesis for Powder-form Intermetallics and Other Compounds. *J. Am. Chem. Soc.* **1961**, *83*, 4916-4919.

(22) Wang, F.; Yao, G.; Xu, M.; Zhao, M.; Zhang, P.; Song, X. Ag-Sb composite prepared by chemical reduction method as new anode materials for lithium-ion batteries.*Mater. Sci. Engineer. B*. **2011**, *176*, 442-445.

(23) Luther, J. M.; Zheng, H.; Sadtler, B.; Alivisatos, A. P. Synthesis of PbS nanorods and other ionic nanocrystals of complex morphology by sequential cation exchange reactions. *J. Am. Chem. Soc*. **2009**, *131*, 16851-16857.

(24) Sines I. T.; Schaak, R. E. Phase-Selective Chemical Extraction of Selenium and Sulfur from Nanoscale Metal Chalcogenides: A General Strategy for Synthesis, Purification, and Phase Targeting. *J. Am. Chem. Soc.* **2011**, *133*, 1294-1297.

(25) Han, S. K.; Gu, C.; Gong, M.; Yu, S. H. A Trialkylphosphine-Driven Chemical Transformation Route to Ag- and Bi-Based Chalcogenides. *J. Am. Chem. Soc*. **2015**, *137*, 5390-5396.

(26) Liang, Q.; Huang, K.; Ren, X.; Zhang, W.; Xie R.; Feng, S. Synthesis of Cu-Sb-S nanocrystals: insight into the mechanism of composition and crystal phase selection. *CrystEngComm*. **2016**, *18*, 3703-3710.

(27) Xu,Y.; Yuan, L.; Xie, R.; Wang, L.; Liang, Q.; Geng, Z.;Liu, H.; Huang, K. Shape Control of Ternary Sulfide Nanocrystals. *Cryst. Growth Des*. **2018**, *18*, 864-871.

(28) Naumkin, A.; Anna Kraut-Vass, V.; Gaarenstroom, S. W.; Powell, C. J. NIST X-ray Photoelectron Spectroscopy Database, NIST Standard Reference Database 20, Version 4.1, **2012.**

(29) Yuan, L.; Huang, K.; Wang, S.; Hou, C.; Wu, X.; Zou, B.; Feng, S. Crystal Shape Tailoring in Perovskite Structure Rare-Earth Ferrites $REFeO_3$ (RE = La, Pr, Sm, Dy, Er, and Y) and Shape-Dependent Magnetic Properties of $YFeO_3$. Cryst. *Growth Des.* **2016**, *16*, 6522-6530.

(30) Wang, S.; Wu, X.; Yuan, L.; Zhang, C.; Lu, D. Shapetuneable synthesis of perovskite structured rare-earth chromites $RECrO_3$via a mild hydrothermal method. *CrystEngComm*. **2017**, *19*, 6436-6442.

(31) van der Stam, W.; Bladt, E.; Rabouw, F. T.; Bals, S.; de Mello Donega, C. Near-Infrared Emitting $CuInSe_2/CuInS_2$ Dot

Core/Rod Shell Heteronanorods by Sequential Cation Exchange. *ACS Nano*. **2015**, *9*, 11430-11438.

(32) Zhang, T.; Schwedtmann, K.; Weigand, J. J.; Doert, T.; Ruck, M. Dissolution behaviour and activation of selenium in phosphonium based ionic liquids. *Chem. Commun.* **2017**, *53*, 7588-7591.

(33) Zhang, T.; Schwedtmann, K.; Weigand, J. J.; Doert, T.; Ruck, M. Understanding the Chemical Reactivity of Phosphonium-Based Ionic Liquids with Tellurium. *Chem. Eur. J.* **2018**, *24*, 9325–9332.

(34) Kaiser, M.; Rasche, B.; Ruck, M. The Topochemical Pseudomorphosis of a Chloride into a Bismuthide. *Angew. Chem. Int. Ed.* **2014**, *53*, 3254–3258.

(35) Kaiser, M.; Baranov, A. I.; Ruck, M. $Bi_2Pt$ ($hP_9$) by Low-Temperature Reduction of $Bi_{13}Pt_3I_7$: Reinvestigation of the Crystal Structure and Chemical Bonding Analysis. *Z. Anorg. Allg. Chem.* **2014**, *640*, 2742–2746.

TOC

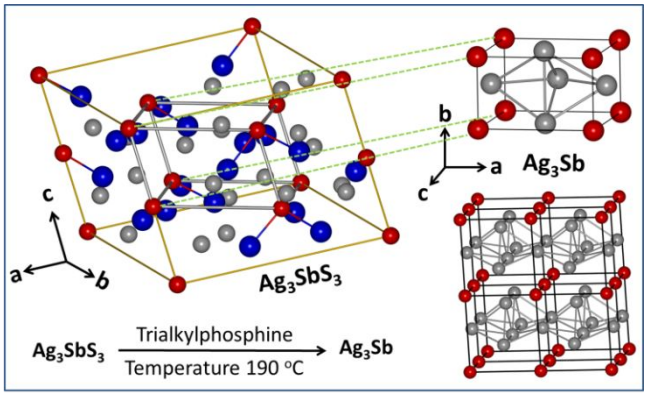
c
a
b
$Ag_3SbS_3$
b
a
c
$Ag_3Sb$
$Ag_3SbS_3$
Trialkylphosphine
Temperature 190 °C
$Ag_3Sb$